Biosurface and Biotribology

WILEY

The Institution of Engineering and Technology

ORIGINAL RESEARCH OPEN ACCESS

One-Step Co-Deposition of Phase-Transited Protein and Zwitterionic Polymers for Robust Antifouling and Lubricious Coatings

Zaiyan Zhang[1] | Yuhang Liu[1] | Pengfei Li[1] | Yuhao Zhang[2] | Jiawen Zhang[2] | Ziqian Zhao[3] | Li Xiang[1]

[1]School of Mechanical Engineering, Jiangsu Key Laboratory for Design and Manufacturing of Precision Medicine Equipment, Southeast University, Nanjing, China | [2]School of Materials Science and Engineering, State Key Laboratory of Engineering Materials for Major Infrastructure, Southeast University, Nanjing, China | [3]School of Materials Science and Engineering, Central South University, Changsha, China

Correspondence: Ziqian Zhao (ziqian.zhao@csu.edu.cn) | Li Xiang (lxiang_me@seu.edu.cn)

Received: 9 March 2026 | **Revised:** 11 June 2026 | **Accepted:** 1 July 2026

Keywords: biomaterials | coatings | lubrication | surface modification

ABSTRACT

Developing protective coatings with desirable antifouling and lubricating capabilities is crucial for the long-term performance of implantable and interventional medical devices. However, stably immobilising functional materials onto diverse substrates without complex pretreatment remains a major challenge. Herein, we report a 'one-step co-deposition' strategy to prepare multifunctional coatings by synergising the amyloid-like phase transition of bovine serum albumin (BSA) with zwitterionic polymers. Phase-transited BSA (PTB), generated via rapid amyloid-like aggregation induced by the reduction of intramolecular disulfide bonds using tris(2-carboxyethyl)phosphine (TCEP), acts as a robust interfacial anchor. This anchor embeds zwitterionic polymers—including poly(sulfobetaine methacrylate) (PSBMA), poly(carboxybetaine methacrylate) (PCBMA) and poly(2-methacryloyloxyethyl phosphorylcholine) (PMPC)—into a dense protein network, realising the rapid functionalisation of various material surfaces (e.g., metals, inorganic ceramics and hydrophobic polymers), forming ultrathin and superhydrophilic coatings. The resulting coatings exhibit outstanding resistance to nonspecific biofouling, inhibiting the adsorption from complex biological fluids, proteins and lipids by over 90%. Also, the strongly hydrated zwitterionic polymers enable an efficient lubrication ability, reducing the friction coefficient to an ultralow range of 0.005–0.015 under physiological conditions. This work presents a facile strategy that simultaneously integrates exceptional antifouling and ultra-lubricating properties, offering great potential for tailoring multifunctional surfaces on biomedical devices for bioengineering applications.

1 | Introduction

Advanced implantable medical devices (IMDs), such as joint prostheses and vascular catheters, require sophisticated surface engineering to maintain long-term stability in physiological environments [1–7]. When foreign materials—including biosensors, catheters and implants—come into contact with biological fluids, they instantaneously trigger the nonspecific adsorption of proteins, subsequently leading to the adhesion of cells or bacteria. This phenomenon, known as 'biofouling', can cause severe complications, including thrombosis, device-associated infections and signal distortion in sensing applications. Concurrently, the high surface friction and wear generated by these devices during insertion or operation can inflict mechanical damage on mucosal tissues, resulting in physiological discomfort [8–14]. Conventional synthetic polymer coatings, such as polyethylene glycol (PEG) [15], can endow

IMD surfaces with antifouling properties in biological fluids via the robust hydration layer formed on the substrate. However, the preparation of these coatings typically entails time-consuming and cumbersome pretreatments for different substrates or involves the use of toxic reagents during synthesis, which compromises biocompatibility and restricts their biomedical applications [16–19]. Therefore, constructing functional interfaces that combine 'ultralow-fouling' capabilities with excellent lubricity is of paramount importance for the development of next-generation medical devices [20].

Among all the approaches developed to fabricate novel antifouling surfaces, the incorporation of zwitterionic polymers exhibits great promise for preventing nonspecific adsorption of biofoulants. Utilising highly hydrated chemical groups with optimal physical properties, coupled with appropriate surface coating techniques, is an effective strategy for developing stable, nonfouling materials for long-term applications [21]. The hydration layers formed by zwitterionic polymers bind water molecules more tightly via electrostatic interactions, thereby enabling these polymers to effectively resist the adhesion of foulants [22–24]. However, the stable immobilisation of these polymers onto diverse substrate materials remains a critical challenge. Natural proteins offer inherent biocompatibility and substrate-independent anchoring capabilities [6, 17, 25, 26]. For instance, native bovine serum albumin (BSA) is widely used as a blocking agent in immunoassays due to its ability to adhere to plastics, metals and glass [27]. Building on this, Hu et al. demonstrated that the rapid reduction of intramolecular disulfide bonds in BSA using tris(2-carboxyethyl)phosphine (TCEP) triggers conformational unfolding and phase transition [28]. The resulting phase-transited BSA (PTB) exposes abundant hydrophobic residues and free thiol groups, enabling it to self-assemble into amyloid-like nanofilms and adhere firmly to virtually any material surface, thereby significantly enhancing its anchoring capacity [28].

Herein, we have developed a facile and universal 'one-step co-deposition' strategy to construct biomedical coatings that combine robust interfacial binding with superior antifouling and lubricating functions [29]. The core of this strategy lies in the synergistic integration of two functional components: zwitterionic polymers—including poly(sulfobetaine methacrylate) (PSBMA), poly(carboxybetaine methacrylate) (PCBMA) and poly(2-methacryloyloxyethyl phosphorylcholine) (PMPC)—with well-defined molecular weights synthesised via reversible addition–fragmentation chain transfer (RAFT) polymerisation, and phase-transited BSA (PTB). The selection of SBMA, CBMA and MPC was based on their representative zwitterionic structures, excellent hydration capability and suitability for controlled polymerisation. These three monomers represent three typical classes of zwitterionic materials, namely sulfobetaine, carboxybetaine and phosphorylcholine, which have been widely recognised as effective nonfouling motifs. Compared with conventional neutral hydrophilic candidates such as poly (ethylene glycol)-based materials, zwitterionic polymers can bind water molecules more strongly through electrostatically induced hydration rather than solely relying on hydrogen bonding or steric repulsion. In addition, the methacrylate structures of SBMA, CBMA and MPC enable well-controlled RAFT polymerisation, allowing polymers with comparable backbones and degrees of polymerisation to be prepared. This provides a suitable platform for comparing the influence of different zwitterionic side-chain structures on coating performance. In addition, SBMA-, CBMA- and MPC-based polymers have been widely explored in biomedical interface engineering and are generally regarded as biofriendly and low-fouling materials for surface modification [30–32]. Their charge-balanced zwitterionic structures and strong hydration capability enable low nonspecific interactions with proteins, cells and biological fluids, which are favourable for maintaining a biologically compatible interface. Therefore, the incorporation of PSBMA, PCBMA and PMPC is not expected to compromise the inherent biocompatibility of the BSA-based coating, but rather to further improve its antifouling performance by constructing a highly hydrated zwitterionic interface. During the TCEP-mediated reduction of disulfide bonds, BSA undergoes amyloid-like aggregation, exposing abundant hydrophobic residues and free thiol groups. This allows it to serve as a 'universal interfacial anchor', firmly adhering to various metallic, inorganic and organic polymeric substrates via multiple noncovalent interactions, thus eliminating the need for tedious chemical pretreatments. Simultaneously, the zwitterionic polymer chains are mechanically entrapped in situ and physically entangled within the dense PTB network, constructing a strongly bound hydration layer at the interface. This hydration shell not only establishes a physical and energetic barrier that effectively inhibits nonspecific adsorption from complex biological fluids (e.g., serum and milk) but also traps water molecules to form a fluid-bearing layer, realising efficient 'hydration lubrication' [33, 34]. This work not only elucidates the synergistic mechanism combining bio-inspired adhesion with synthetic polymer functionality but also provides a rapid, scalable and universal solution for the surface functionalisation of implantable and interventional medical devices.

2 | Materials and Methods

2.1 | Materials

Bovine serum albumin (BSA, ≥ 98%) and tris(2-carboxyethyl) phosphine (TCEP, ≥ 98%) were purchased from Shanghai Macklin Biochemical Co. Ltd (Shanghai, China). The zwitterionic monomers, including [2-(methacryloyloxy)ethyl]dimethyl-(3-sulfopropyl)ammonium hydroxide (SBMA, ≥ 98%), 2-carboxy-N, N-dimethyl-N-(2′-methacryloyloxyethyl)ethanaminium inner salt (CBMA, ≥ 98%) and 2-methacryloyloxyethyl phosphorylcholine (MPC, ≥ 98%), were all obtained from Macklin (Shanghai, China). For the reversible addition–fragmentation chain transfer (RAFT) polymerisation, 4-cyano-4-(phenylcarbonothioylthio)pentanoic acid (≥ 98%) and 4,4′-azobis (4-cyanovaleric acid) (ACVA, ≥ 98%) were selected as the chain transfer agent (CTA) and the radical initiator, respectively, both from Macklin. Fluorescein isothiocyanate (FITC)-labelled conjugates, including BSA-FITC, HSA-FITC and Dextran-FITC, were obtained from Solarbio Science & Technology Co. Ltd. (Beijing, China). Fetal bovine serum (FBS) was purchased from Biosharp

(Hefei, China), whereas fresh milk, egg yolk and egg white were acquired from a local grocery store. Model proteins and enzymes, specifically Concanavalin A (Con A, ≥ 96%), collagenase (CLG, ≥ 96%), lysozyme (Lyso, ≥ 96%) and mucin (≥ 96%), were all purchased from Shanghai Macklin Biochemical Co. Ltd. (Shanghai, China). Gold substrates (Au substrates) were supplied by Nanjing Jingchenshun System Technology Co. Ltd. (Nanjing, China). Silicon wafers were supplied by Juancheng Lilengke Electronic Accessories Co. Ltd. (China). Mica was purchased from Nanjing Runtang Trading Co. Ltd. (Nanjing, China). All chemicals and solvents were used as received without further purification. Deionised water (DW) was produced using a Milli-Q Integral 3 system (EMD Millipore; resistivity, 18.2 MΩ·cm; total organic content < 3 ppb).

2.2 | Preparation of Phase-Transited BSA and Zwitterionic Polymer Co-Deposited Coatings

2.2.1 | Preparation of Phase-Transited BSA and Zwitterionic Polymers

As illustrated in Figure 1a, PTB was prepared by reducing native BSA with TCEP. Briefly, 100 mg of BSA was dissolved in 10 mL of deionised water, followed by the addition of 10 mL of TCEP solution (10 mg mL^{-1}), with the pH adjusted to 6.0 using NaOH. The mixture was sealed in a glass vial and stirred magnetically for 30 min. To remove unreacted reagents, the resulting solution was purified by dialysis against deionised water for 3 days. Finally, the product was collected as a PTB powder after lyophilisation.

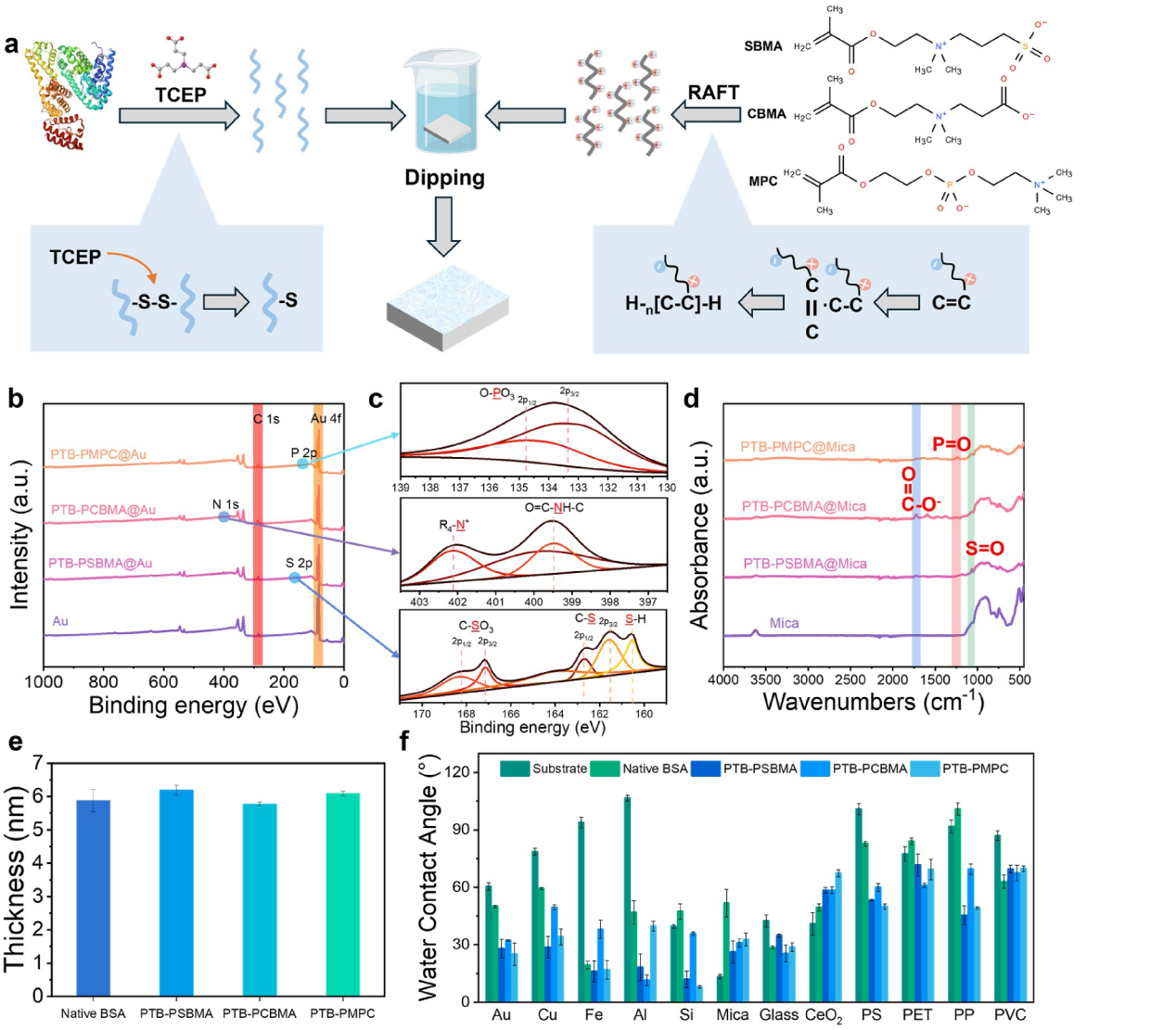

FIGURE 1 | Preparation and characterisation of the BSA-based coatings. (a) Schematic illustration of the preparation of PTB via TCEP reduction, the synthesis of zwitterionic polymers through RAFT polymerisation and the facile one-step co-deposition process of PTB and zwitterionic polymers for surface functionalisation. (b) XPS survey spectra of pristine Au and Au surfaces modified with PTB-PSBMA, PTB-PCBMA and PTB-PMPC. (c) Corresponding high-resolution deconvolution spectra of S 2p, N 1s and P 2p, confirming the successful conjugation of various functional components. (d) FTIR spectra of bare mica and mica surfaces modified with PTB-PSBMA, PTB-PCBMA and PTB-PMPC. (e) Coating thickness of different functionalised surfaces measured by spectroscopic ellipsometry. (f) Static water contact angles on different surfaces, demonstrating the variation in surface hydrophilicity after modification.

Target zwitterionic polymers, including poly(sulfobetaine methacrylate), poly(carboxybetaine methacrylate) and poly(2-methacryloyloxyethyl phosphorylcholine), with a degree of polymerisation (DP) of 200 were synthesised via reversible addition-fragmentation chain transfer (RAFT) polymerisation [35, 36], as also depicted in Figure 1a. Specifically, zwitterionic monomers (SBMA, CBMA or MPC, 5 mmol), the chain transfer agent (0.025 mmol) and the initiator (0.02 mmol) were dissolved in 15 mL of 0.5 M NaCl solution. The reaction mixture was purged with nitrogen gas for 30 min to eliminate dissolved oxygen. Subsequently, the polymerisation was conducted at 70°C for 24 h. The resulting polymer solution was purified by dialysis against deionised water for 3 days to remove unreacted monomers and impurities, followed by lyophilisation to obtain the final zwitterionic polymers.

2.2.2 | *Preparation of Co-Deposited Coatings*

Co-deposited coatings were fabricated on various substrates, including metallic, inorganic and organic materials, via a facile one-step co-deposition strategy [37–39]. Taking the gold (Au) substrate as a representative example, the Au substrate was first pretreated by irradiation in an ultraviolet (UV) ozone cleaner for 20 min to remove surface contaminants. A total of 20 mg of lyophilised PTB powder was dispersed in 10 mL of PBS buffer (50 mM, pH 8.5) and ultrasonicated for 30 min in an ice-water bath. Subsequently, 20 mg of a zwitterionic polymer (PSBMA, PCBMA or PMPC) was added to the solution and thoroughly mixed to obtain a co-deposition dispersion. The pretreated Au substrates were then immersed in the dispersion at room temperature for 10 h under constant orbital shaking at 50 rpm. Finally, the functionalised substrate was removed, thoroughly rinsed with ultrapure water to eliminate loosely bound molecules, and dried under a stream of nitrogen gas to obtain the PTB and Zwitterionic Polymer Co-Deposited Coating.

2.3 | Characterisation

2.3.1 | *Material Characterisation*

UV-Vis absorption spectra were recorded using a Shimadzu UV-2600 spectrophotometer (Japan) in the wavelength range of 250–500 nm to characterise the standard calibration curve of native BSA, the Ellman's reaction in different solutions and the reduction kinetics of BSA by TCEP. First, a standard calibration curve for BSA in TE buffer (50 mM Tris-HCl, 1 mM EDTA, pH 7.5) was established, as shown in Supporting Information S1: Figure S1. The concentration of free thiol groups in the solution was determined via the classical Ellman's assay. Specifically, 50 μL of Ellman's reagent solution (4 mg mL^{-1}) was mixed with 2.5 mL of the sample solution and incubated at room temperature for 15 min prior to spectral acquisition. To prevent the interference of TCEP with Ellman's reagent during quantitative analysis, residual TCEP in the BSA solution was removed using a desalting column. As shown in Supporting Information S1: Figure S2, the desalting process effectively eliminated interference from TCEP, thereby ensuring the accurate detection of thiol groups in the PTB solution. In addition, the reduction of BSA by TCEP over different reaction times was monitored and summarised (Supporting Information S1: Figure S3). The results indicate that TCEP rapidly reduces BSA, with the reaction reaching equilibrium within approximately 15 min. For the zwitterionic polymers, their chemical structures were characterised by Fourier transform infrared (FTIR) spectroscopy using a Thermo Fisher Nicolet iS50 spectrometer over the wavenumber range of 500–4000 cm^{-1} (Supporting Information S1: Figure S4). The molecular weights of the synthesised polymers were determined by gel permeation chromatography (GPC) using an Agilent 1260 Infinity II system (USA), with detailed results provided in Supporting Information S1: Table S1.

2.3.2 | *Surface Characterisation*

To confirm the successful co-deposition of PTB and zwitterionic polymers on the substrates, FTIR spectra of bare mica and mica surfaces modified with PTB-PSBMA, PTB-PCBMA and PTB-PMPC were recorded using a Thermo Fisher Nicolet iS50 spectrometer (USA) in the wavenumber range of 500–4000 cm^{-1}. The chemical composition of the coatings on different substrates was analysed by X-ray photoelectron spectroscopy (XPS) using a Thermo Scientific K-Alpha spectrometer (USA). Survey scans were collected over a binding energy range of 0–1000 eV, followed by high-resolution scans for S, N and P elements. The thickness of native BSA, PTB-PSBMA, PTB-PCBMA and PTB-PMPC coatings on silicon wafers (Si) was determined using a spectroscopic ellipsometer (J.A. Woollam RC2, USA). Surface wettability was evaluated by measuring the static water contact angle (WCA) using a contact angle goniometer (Ossila L2004A1, UK). Furthermore, the surface morphology of pristine Au and polymer-modified Au surfaces (PTB-PSBMA@Au, PTB-PCBMA@Au and PTB-PMPC@Au) was characterised by atomic force microscopy (AFM) in AC mode under dry conditions using AC240 probes. The surface roughness was quantified by the root-mean-square (RMS) value.

2.3.3 | *Fluorescence-Based Static Biofoulant Adsorption Assay*

The adsorption behaviours of BSA-FITC, HSA-FITC and Dextran-FITC on pristine mica, native BSA@Mica and PTB-zwitterionic polymer-modified mica surfaces (PTB-PSBMA@-Mica, PTB-PCBMA@Mica and PTB-PMPC@Mica) were qualitatively determined using an Olympus IX71 inverted fluorescence microscope (Japan). Specifically, both the pristine and modified mica substrates were immersed in PBS buffer (1×, pH 7.4) containing the respective fluorescent probes at a concentration of 0.1 mg mL^{-1}. The samples were incubated for 12 h in the dark. Subsequently, the surfaces were thoroughly rinsed with fresh PBS buffer to eliminate loosely bound foulants prior to fluorescence imaging.

2.3.4 | *Quartz Crystal Microbalance With Dissipation Monitoring (QCM-D) Test*

In this assay, diluted biofluids (5%) and protein solutions (10 mg mL^{-1}) were employed as model foulants. For the lipid fouling test, canola oil—selected as a model lipid due to its high viscosity—was dissolved in ethanol and sonicated for 30 min. The lipid/ethanol mixture was subsequently dispersed in water using a high-shear homogeniser (T18 digital ULTRA-TURRAX, IKA, Germany) at 20,000 rpm for 15 min to form a stable emulsion. To prepare the functionalised sensors, bare Au sensors were immersed in the co-deposition dispersion at room

temperature for 10 h. All QCM-D measurements were performed using a Gamry QCM-I Mini instrument (USA). The obtained data were analysed based on the extended viscoelastic model using the Biosense software [7, 40, 41].

2.3.5 | *Chemical Mapping Analysis via O-PTIR*

To evaluate the antifouling performance of the BSA-based coatings, bare substrates, native BSA-modified substrates and PTB-zwitterionic polymer-coated substrates (PTB-PSBMA, PTB-PCBMA and PTB-PMPC) were incubated in various fouling solutions—including egg white, FBS, milk and lipids—at 37°C for 24 h. Specifically, gold substrates were employed for the fouling assays involving proteins, FBS and milk, whereas silicon wafers were utilised for the lipid fouling tests. Following the 24 h incubation period, the substrates were removed and thoroughly rinsed with extensive ultrapure water to eliminate loosely adherent foulants prior to characterisation.

2.3.6 | *Tribological Measurements*

Tribological tests were conducted using a UMT TriboLab tribometer (Bruker, USA) in a linear reciprocating ball-on-disk configuration. A polytetrafluoroethylene (PTFE) ball with a diameter of 5 mm was employed as the upper counterpart. Prior to the measurements, the PTFE ball was sequentially ultrasonicated in acetone, ethanol and pure water, followed by drying under a stream of nitrogen gas. The pristine and surface-modified silicon substrates were mounted in a Petri dish (diameter = 50 mm) to serve as the stationary lower plate. To simulate physiological conditions, PBS buffer (1×, pH 7.4) was added to the dish, ensuring that the substrates were fully immersed in the solution. The applied normal load (F_n) ranged from 0.1 to 20 N. For the linear reciprocating motion, the stroke length was fixed at 5 mm, whereas the average sliding velocity (v_s) varied from 0.5 to 10 mm s^{-1}.

3 | Results and Discussion

3.1 | One-Step Preparation and Fundamental Properties of PTB–Zwitterionic Polymer Co-Deposited Coatings

The construction of the multifunctional nanocoating was accomplished through a simple one-step co-deposition strategy that integrates the phase-transition behaviour of BSA with the specific chemical functionalities of zwitterionic polymers. As illustrated in Figure 1a, native BSA was first reduced by TCEP. This reduction cleaves the intramolecular disulfide bonds, inducing protein unfolding and thereby exposing hydrophobic residues and free thiol groups that facilitate surface anchoring. The reduction process was verified by UV-Vis spectroscopy [5]. Following TCEP treatment, the characteristic absorbance at 412 nm corresponding to the chromogenic reaction between Ellman's reagent and thiol groups increased markedly (Supporting Information S1: Figures S1–S3), confirming the successful generation of free thiols.

Meanwhile, three distinct zwitterionic polymers—PSBMA, PCBMA and PMPC—were synthesised via reversible addition–fragmentation chain transfer (RAFT) polymerisation [36]. Their chemical structures were confirmed by FTIR spectroscopy (Supporting Information S1: Figure S4), which exhibited characteristic vibrational bands of sulfonate groups, quaternary ammonium moieties and phosphate groups [42]. GPC analysis (Supporting Information S1: Table S1) demonstrated well-controlled molecular weights and narrow polydispersity indices, which are favourable for the formation of uniform polymer brush layers [43]. Leveraging the strong anchoring capability of PTB, the zwitterionic polymers were entrapped within a densely packed protein network, and co-deposition was achieved via a straightforward one-step dip-coating process.

The surface chemical composition of the resulting coatings on gold substrates was characterised by XPS. The survey spectra (Figure 1b, Supporting Information S1: Figure S5) revealed a clear transition from Au-dominated signals of the pristine substrate to spectra enriched in C, N and O, indicating complete surface coverage. High-resolution core-level spectra (Figure 1c) further confirmed the successful incorporation of the three zwitterionic polymers, clearly identifying the characteristic chemical environments of each functional component. Specifically, the S 2p spectrum of the PTB-PSBMA coating displayed a high-binding-energy peak attributed to sulfonate groups ($-SO_3^-$), confirming the presence of sulfobetaine side chains [44]. For the PTB-PCBMA surface, the N 1s spectrum exhibited a distinct signal corresponding to quaternary ammonium groups ($-N^+(CH_3)_3$), distinguishable from the amide nitrogen of the protein backbone [45]. In the case of the PTB-PMPC coating, the P 2p spectrum clearly identified the characteristic peak of phosphate ester groups (P = O), explicitly validating the successful co-deposition of the phosphorylcholine functionality [46]. These findings were further corroborated by FTIR analysis on mica substrates (Figure 1d), where, in addition to the amide bands of the protein network, the characteristic stretching vibrations of sulfonate (S = O, 1040 cm^{-1}), carboxylate (COO^-, 1600 cm^{-1}) and phosphate (P = O, 1240 cm^{-1}) groups were clearly observed [45–48].

A critical advantage of this co-deposition strategy lies in its substrate universality. As evidenced by the static water contact angle (WCA) measurements (Figure 1f, Supporting Information S1: Figure S6), the co-deposition process consistently transformed a diverse library of substrates—ranging from metals and inorganic ceramics to hydrophobic polymers—into superhydrophilic surfaces with WCAs typically dropping below 20°. Spectroscopic ellipsometry [49] (Figure 1e) indicated that these functional coatings are ultrathin, with an average thickness of approximately 5–6 nm, ensuring minimal dimensional change to the underlying devices. Furthermore, Atomic Force Microscopy (AFM) characterisation was performed to further evaluate the surface microstructure of the functional coatings (Figure 2a). The pristine Au surface exhibited an atomically flat morphology with a low RMS roughness of 0.190 nm. After co-deposition, the PTB-PSBMA, PTB-PCBMA and PTB-PMPC coatings displayed continuous and homogeneous nanoscale granular morphologies, which are typical of amyloid-like protein aggregation [50]. The corresponding 3D AFM topographic images further confirmed the formation of dense coating layers without obvious cracks or large-scale defects. The RMS roughness values of PTB-PSBMA, PTB-PCBMA and PTB-PMPC were 0.967, 0.992 and 0.706 nm, respectively, indicating that the coatings introduced only slight nanoscale roughness while

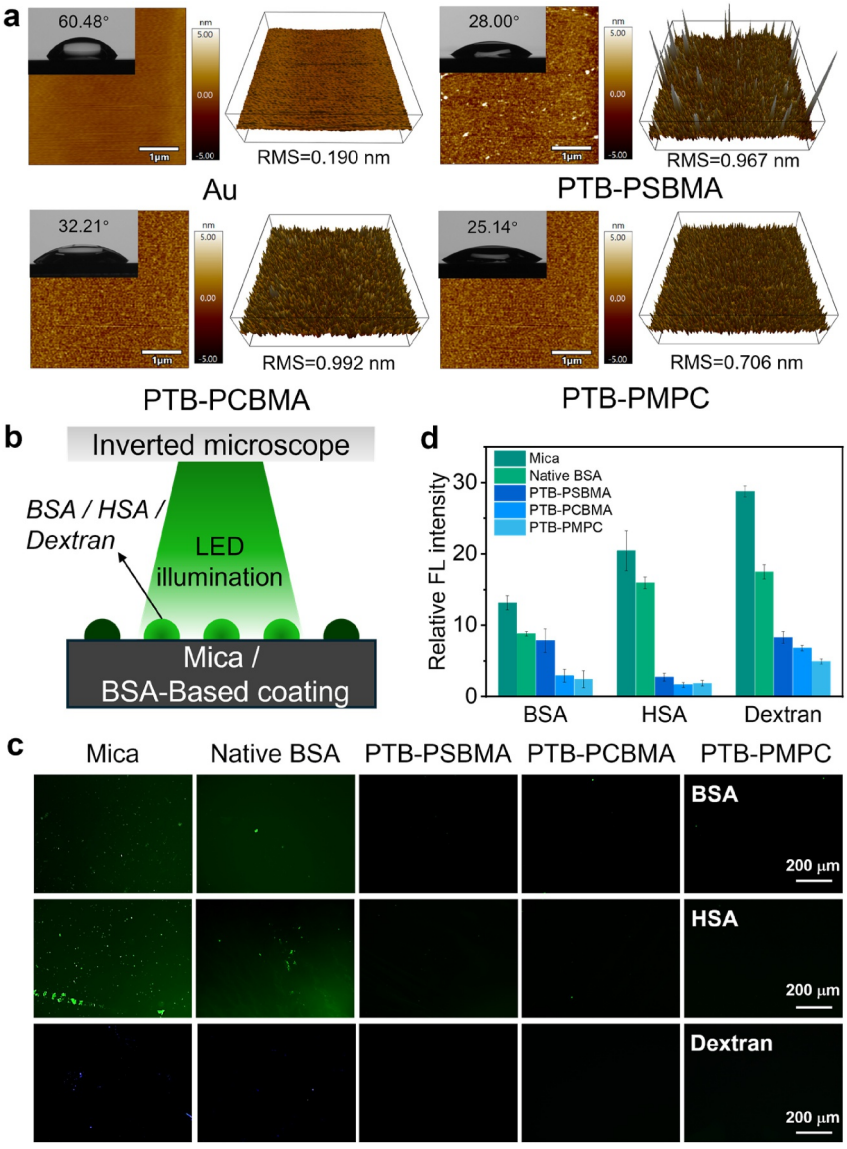

FIGURE 2 | Surface morphology of the modified substrates and observation of biofoulant adsorption on different surfaces. (a) AFM height images, corresponding 3D topographic images, water contact angles and RMS roughness values of pristine Au, PTB-PSBMA@Au, PTB-PCBMA@Au and PTB-PMPC@Au surfaces. (b) Schematic illustration of the experimental principle for observing biofoulant adsorption on the surfaces by fluorescence microscopy. (c) Fluorescence images showing the distribution of biofoulants on pristine mica, PTB-PSBMA@Mica, PTB-PCBMA@Mica and PTB-PMPC@Mica (scale bar = 200 μm). (d) Quantitative analysis of relative fluorescence intensities derived from the corresponding fluorescence images.

maintaining relatively smooth surface features. In addition, the height profiles shown in Supporting Information S1: Figure S9 revealed that the surface height fluctuations were mainly confined within several nanometres, further supporting the uniform and continuous microstructure of the coatings. Such a nanoscale and defect-free coating morphology provides a stable structural foundation for maintaining hydration layers, thereby benefiting the subsequent antifouling and lubrication applications.

3.2 | Antifouling Performance of PTB–Zwitterionic Polymer Co-Deposited Coatings

The antifouling mechanism depends on the synergistic action between PTB and the zwitterionic moieties. PTB presents a variety of functional groups—including amino, carboxyl, hydroxyl, thiol, amide and hydrophobic carbonaceous motifs—that strongly bind and immobilise the zwitterionic polymers. The zwitterionic groups (sulfobetaine, carboxybetaine and phosphorylcholine) possess large electrostatic dipole moments and tightly coordinate a dense, energetically favourable hydration layer [48, 51]. This physical and energetic water barrier imposes substantial steric hindrance and a large thermodynamic penalty on the adsorption of diverse biomolecules, effectively preventing their contact with the underlying substrate. To rigorously evaluate this capability, we employed a multiscale assessment comprising microscopic fluorescence imaging, real-time dynamic monitoring and macroscopic chemical imaging. At the microscale, resistance to nonspecific adsorption was directly visualised by fluorescence microscopy [33, 52]. Substrates were incubated with FITC-labelled model foulants representing different classes of biological contaminants:

BSA (a typically negatively charged plasma protein), HSA (Human Serum Albumin) and dextran (a neutral, adhesive polysaccharide). As shown in Figure 2c, the pristine mica and native BSA-modified control surfaces exhibited intense fluorescence after exposure to all three foulants, indicating substantial accumulation. This observation implies that although native BSA is amphiphilic, its hydration capacity is insufficient to repel these foulants. In sharp contrast, surfaces modified with PTB-PSBMA, PTB-PCBMA and PTB-PMPC appeared nearly dark and were visually indistinguishable from the background. Quantitative analysis of the relative fluorescence intensity (Figure 2d) further confirmed that, compared with the blank control group, the adsorption of both proteins and polysaccharides on the zwitterionic-coated surfaces was reduced by more than 60%. This broad-spectrum repellency, independent of foulant charge or size, supports the generality of the hydration-barrier mechanism [24, 41].

Fouling in biological systems—defined as the spontaneous, dynamic adsorption and accumulation of biomolecules on surfaces—can be monitored directly and in real time by quartz crystal microbalance with dissipation monitoring (QCM-D) [41]. The schematic illustration of the working principle of QCM-D is shown in Figure 3a. QCM-D was used to screen the antifouling performance of the PTB-zwitterion co-deposited coatings against a variety of model biological foulants, with bare Au sensors and native BSA-coated Au sensors serving as controls. Figure 3b shows the frequency shifts (ΔF) of the sensors during five cycles of milk–water rinsing. The bare Au sensor exhibited a rapid and large frequency decrease that did not recover after water rinsing, indicating the formation of a thick, irreversibly bound fouling layer. By contrast, the PTB–zwitterionic polymer—functionalised sensors—displayed a markedly different response: although a frequency change was observed during milk injection (attributable to the bulk viscosity of the fluid), the signal returned almost entirely to baseline after rinsing with water. This 'reversible adsorption' behaviour indicates that foulants could not penetrate the hydration shell to form permanent contact with the surface, demonstrating the excellent antifouling performance of the PTB–zwitterion coatings [41]. The PTB–zwitterion coatings showed efficient resistance against a broad spectrum of biological contaminants, including complex biofluids (fetal bovine serum, egg white and egg yolk), common proteins (Concanavalin A, lysozyme, collagenase, BSA and mucin) and lipids (Figure 3c–f, Supporting Information S1: Figure S7). For all three zwitterionic coatings, the irreversibly adsorbed mass was consistently suppressed to negligible levels, typically below 80 ng cm^{-2} (with the exception of egg yolk). For instance, the residual amounts of egg white on PTB-PSBMA, PTB-PCBMA and PTB-PMPC-coated sensors after water rinsing were approximately 15.99, 28.79 and 7.95 ng cm^{-2}, respectively. In stark contrast, the adsorption of egg white on native BSA-coated and bare gold sensors reached significantly higher levels of $\approx$ 1154.15 and $\approx$ 1544.2 ng cm^{-2}, respectively.

Long-term operation using real biofluids in macro-scale bulk tests is of significant practical importance for evaluating the antifouling capacity of coatings. In macro-scale tests, the surfaces undergo more complex physicochemical and biological processes, such as the formation of biofilms, which is the primary cause of irreversible functional failure in devices and healthcare-associated infections. This evaluation was coupled with Optical Photothermal Infrared (O-PTIR) chemical imaging. Although traditional infrared microscopy is typically diffraction-limited, O-PTIR enables the precise localisation of foulants based on their characteristic infrared (IR) peaks, achieving chemical imaging at the submicron scale [53–56]. After being incubated in dilutions of egg white, milk, FBS and lipids for 24 h, the substrates were rinsed with deionised water (Figure 4a). The accumulation of foulants on the substrate surfaces was tracked by monitoring the intensity of their characteristic IR peaks (Figure 4b, Supporting Information S1: Figure S8). The resulting chemical maps (Figure 4c) provided a vivid contrast: the unmodified substrates were heavily blanketed with large, dense aggregates of biomolecules, appearing as high-intensity 'hot spots' across the entire scan area. Conversely, the chemical maps for the PTB-PSBMA, PTB-PCBMA and PTB-PMPC surfaces were predominantly uniform and low-intensity, confirming that the surfaces remained chemically clean. The normalised fouling coverage calculated from these maps (Figure 4d) revealed that although the control surfaces were nearly 100% covered by foulants, the zwitterionic coatings maintained a fouling coverage close to 0%. This result is particularly significant as it proves that the coatings can withstand long-term, static immersion in high-concentration biological fluids without saturation or failure of the antifouling mechanism [24, 28].

The molecular structures of the three zwitterionic polymers may further influence their antifouling behaviours. PSBMA contains a quaternary ammonium cation and a sulfonate anion, in which the sulfonate group remains strongly ionised over a wide pH range, thus providing stable electrostatically induced hydration. PCBMA consists of a quaternary ammonium cation and a carboxylate anion; the carboxylate group can participate in additional hydrogen bonding and electrostatic interactions, although its ionisation state may be more sensitive to environmental pH. PMPC contains a phosphorylcholine group that mimics the hydrophilic headgroup of cell membrane phospholipids, which is beneficial for reducing nonspecific protein and lipid adhesion. Despite these structural differences, all three polymers possess charge-balanced zwitterionic groups and can form tightly bound hydration layers, thereby effectively suppressing the adsorption of proteins, polysaccharides, lipids and complex biological fluids.

3.3 | Lubrication Performance of PTB–Zwitterionic Polymer Co-Deposited Coatings

Beyond their exceptional antifouling properties, the prepared coatings were investigated for their ability to modify surface tribology. In biological systems, such as articular cartilage, lubrication is mediated by surface-bound macromolecules (like lubricin and hyaluronic acid) that trap water to form a fluid load-bearing layer. Mimicking this 'hydration lubrication' mechanism, the zwitterionic polymer chains in our coatings are designed to act as efficient boundary lubricants [57, 58]. To evaluate this, we conducted rigorous tribological testing using a ball-on-disk tribometer under physiological conditions (1 $\times$ PBS, pH 7.4), as illustrated in Figure 5a. As illustrated in Figure 5b, the bare silicon substrate exhibited high and

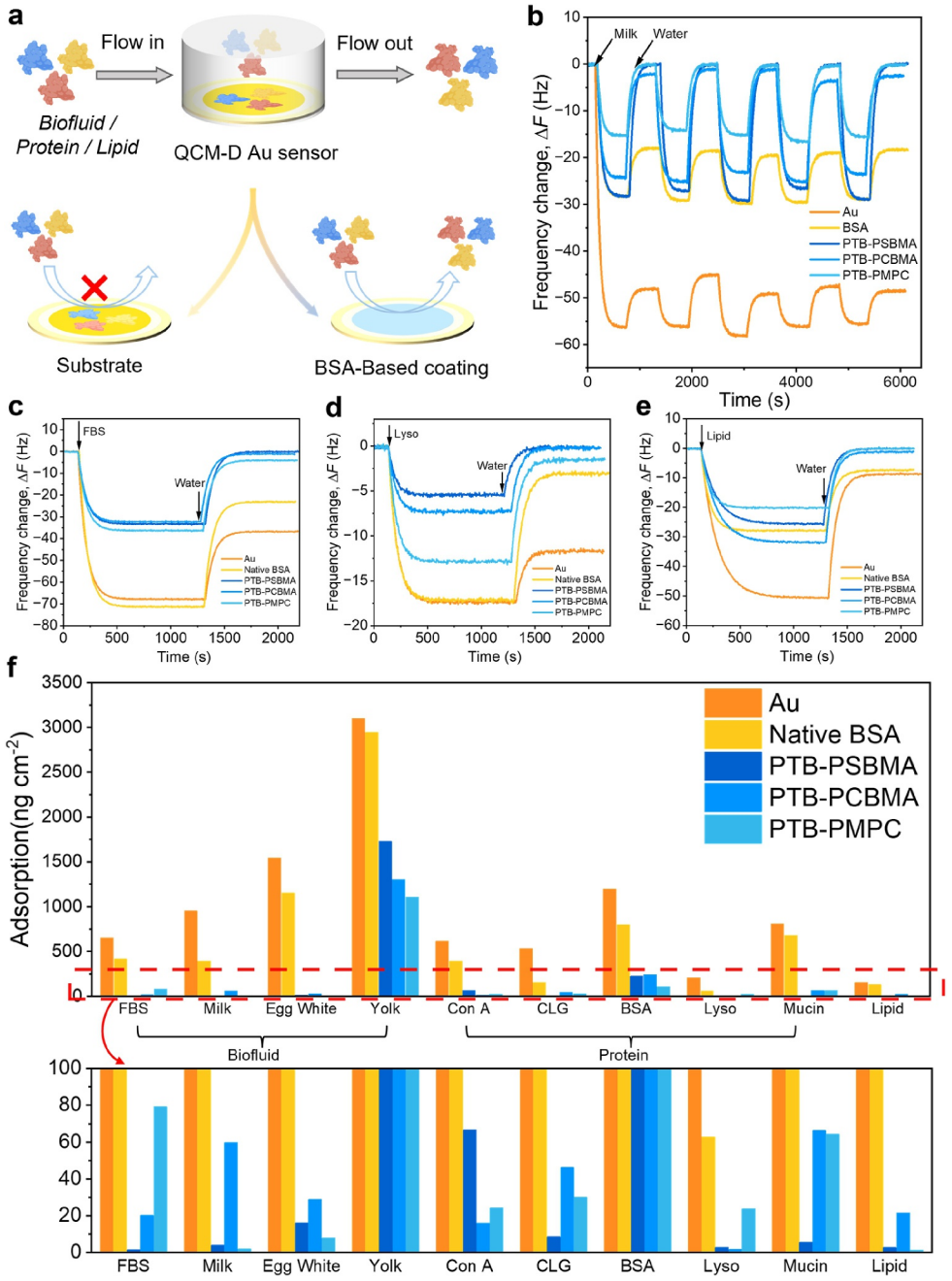

FIGURE 3 | The antifouling performance of the coatings was monitored in real-time and quantitatively evaluated via QCM-D. (a) Schematic illustration of the dynamic adsorption process of biofoulants on the sensor surfaces. (b) Frequency shifts of sensors with different coatings during alternating rinsing cycles of milk and water. (c–e) Corresponding frequency shifts on various modified surfaces during the adsorption of (c) fetal bovine serum (FBS), (d) lysozyme and (e) lipids. (f) Comparison of the residual adsorbed mass of biofluids, proteins and lipids on pristine Au, native BSA-modified surfaces and various PTB–zwitterionic polymer-functionalised surfaces (PTB-PSBMA, PTB-PCBMA and PTB-PMPC) after water rinsing (all data were recorded following the water rinsing step).

significantly fluctuating friction curves with a friction coefficient (μ) exceeding 0.025. This behaviour indicates the occurrence of direct solid–solid asperity contact, which typically leads to high shear stress and surface damage. Although the native BSA coating reduced friction to some extent ($\mu \approx 0.02$), the hydration capacity of the protein layer alone was insufficient to provide efficient lubrication. In contrast, the three PTB–zwitterionic polymer co-deposited coatings all exhibited stable, ultra-low friction coefficients within the range of 0.005–0.015, representing a reduction of approximately 60%–80% compared to the bare substrate. This superior lubricity stems from the robust ability of zwitterions to entrap water molecules. Under normal compression and shear, the resulting hydration layer is tightly bound by strong electrostatic interactions, resisting being squeezed out of the contact zone. This maintains the integrity of the hydration layer and ensures persistent and stable lubrication in physiological aqueous environments [33].

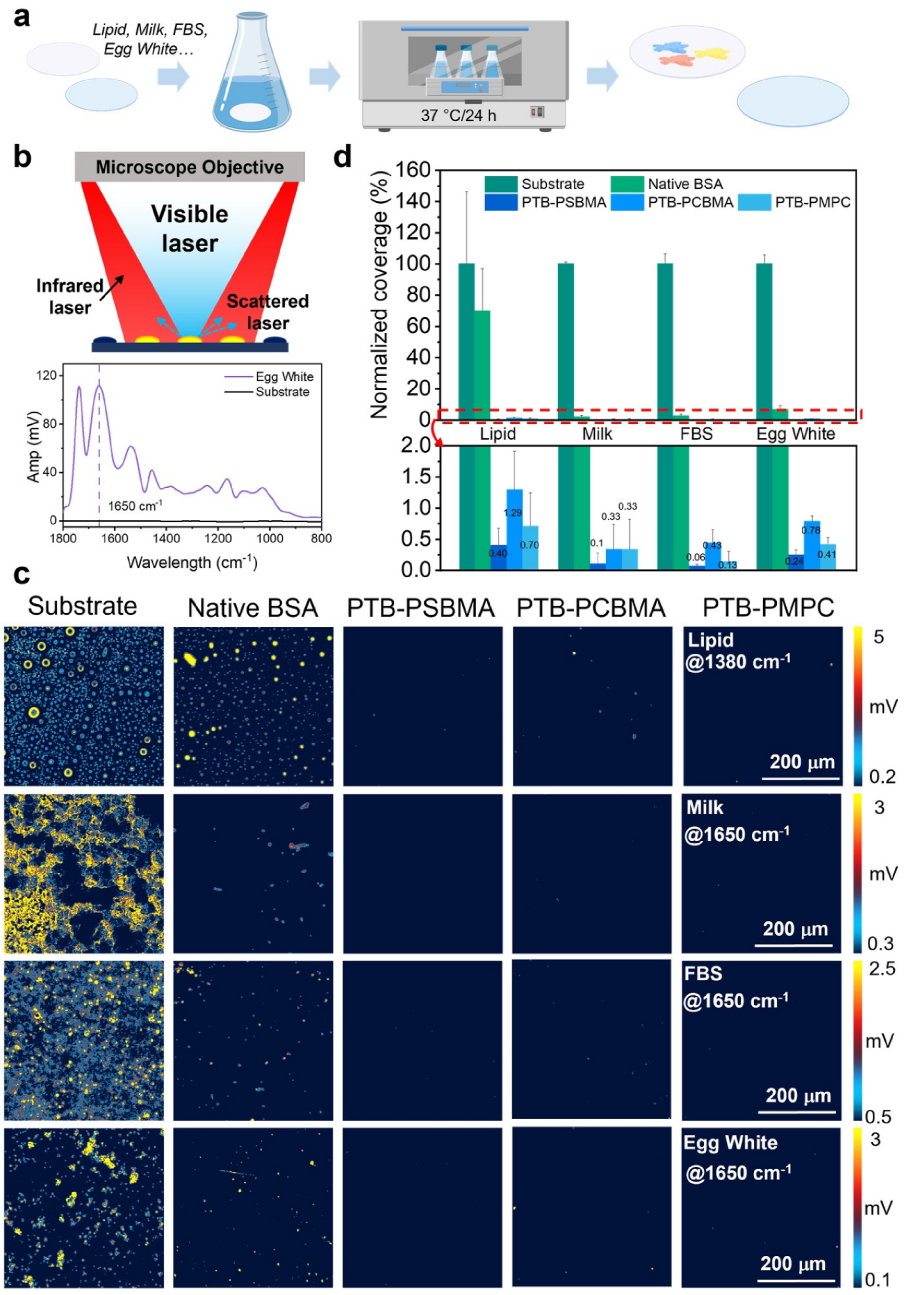

FIGURE 4 | Antifouling performance of the functionalised coatings in bulk fouling tests. (a) Schematic illustration of the experimental workflow for the macroscale bulk fouling tests. (b) Working principle of O-PTIR spectroscopy, and the characteristic O-PTIR spectra of the bare substrate and biofoulants in egg white. (c) O-PTIR Mapping images of biofoulants on the surfaces of pristine substrate, native BSA-modified substrate and various PTB-zwitterionic polymer-functionalised (PTB-PSBMA, PTB-PCBMA and PTB-PMPC) substrates. (d) Corresponding fouling coverage on the aforementioned surfaces after incubation in lipid, milk, FBS and egg white. Values in (d) represent the mean and the standard deviation ($n = 3$).

The lubrication performance of the PTB–zwitterionic co-deposited coatings was further evaluated by measuring the friction between a PTFE probe and the coatings under varying applied loads (F_n) and sliding speeds (v_s) in a physiological aqueous environment. Figure 5c presents the influence of normal load on the frictional behaviour of the multifunctional nanocoatings at a constant sliding speed of 5 mm s^{-1}. As the load was incrementally increased from 0.1 to 20 N (corresponding to a contact stress increase from 10.72 to 62.72 MPa), the μ values remained consistently stable at approximately 0.015. Notably, even under the highest load of 20 N (62.72 MPa), the superlubricating capability was maintained, reaching levels comparable to the lubrication performance found in biotribological systems and confirming its feasibility for various in vivo biotribological applications. Furthermore, the friction coefficients of the PTB–zwitterionic co-deposited coatings were investigated at different sliding speeds (Figure 5d). As the sliding speed increased from 0.5 mm·s^{-1}–10 mm·s^{-1}, μ remained at a low level with negligible variation. This speed-insensitive lubrication behaviour conforms to Amontons' law, further extending the applicability of these coatings to complex scenarios, such as vascular grafts where inner-wall lubrication

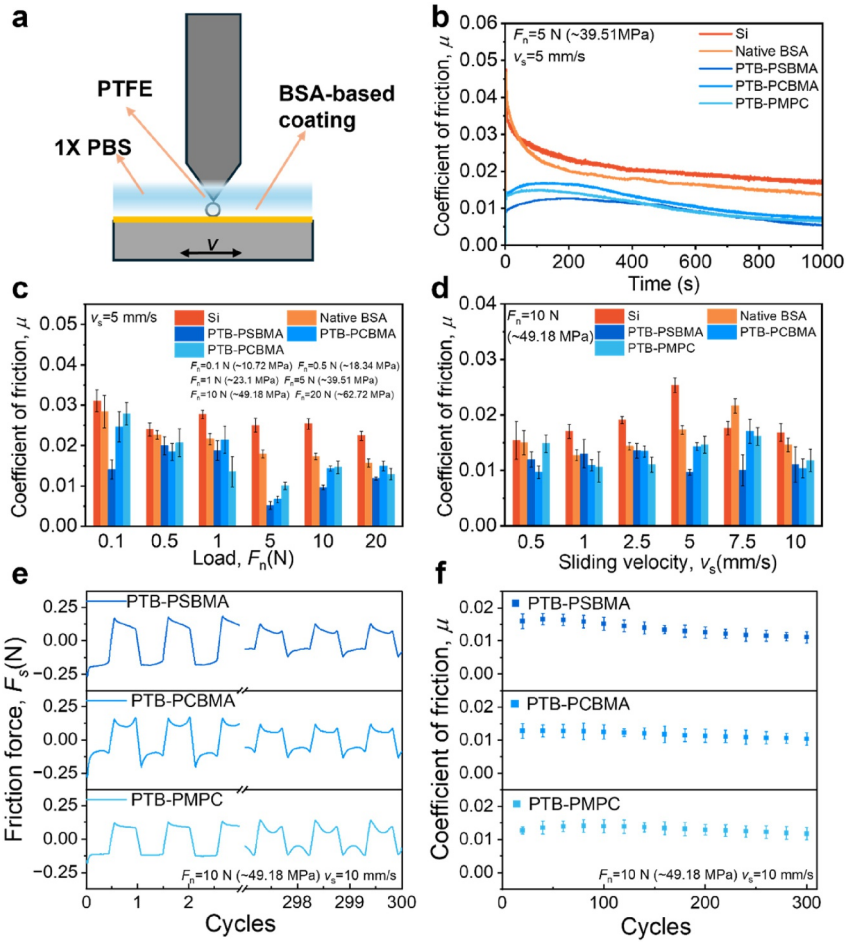

FIGURE 5 | Evaluation of the tribological performance of BSA-based coatings under model physiological aqueous conditions. (a) Schematic illustration of the experimental configuration for friction and wear tests between BSA-based coatings and a PTFE counterpart using a reciprocating tribometer in PBS buffer (1×, pH 7.4). (b) COF-time curves for different modified surfaces. (c) Variation of the friction coefficient μ as a function of the normal load F_n at a constant sliding velocity of 5 mm s^{-1}. (d) Friction coefficient μ versus sliding velocity v_s under a constant normal load of 10 N (49.18 MPa). (e, f) Results of cyclic reciprocating friction tests estimating the lubrication durability of PTB–zwitterionic polymer coatings under a high normal load of 10 N (49.18 MPa) and a sliding velocity of 10 mm s^{-1}.

must be maintained to reduce resistance to blood flow at both low (artificial veins) and high (artificial arteries) velocities [59].

Finally, the long-term durability and wear resistance of the coatings were tested under aggressive conditions ($F_n = 10\,N$, corresponding to a contact stress of 49.18 MPa, and $v_s = 10\,\text{mm}\,\text{s}^{-1}$) for 300 reciprocating cycles. Durability is a critical parameter for biomedical coatings, as delamination or wear-through can lead to device failure or inflammatory responses. As shown in Figure 5e, the friction force curves for the PTB-PSBMA, PTB-PCBMA and PTB-PMPC coatings remained stable, symmetric and low throughout the 300 cycles, with steady-state friction forces ranging from 0.1 to 0.2 N and negligible dependence on the cycle number. After 300 reciprocating cycles, the calculated μ showed almost no change, remaining at approximately 0.015 (Figure 5f), demonstrating a durable lubrication performance comparable to natural hydration lubrication systems [60]. This exceptional mechanical stability is attributed to the synergistic architecture of the coating: (1) the amyloid-like PTB network serves as a robust multipoint anchoring layer that adheres firmly to the substrate, preventing shear-induced delamination; and (2) the zwitterionic polymer chains dissipate shear energy through hydration lubrication. This dual-functional design ensures that the coating maintains its integrity and functional performance even under sustained mechanical stress, making it highly suitable for applications involving moving parts or insertion forces, such as catheters, endoscopes and guidewires [61]. The combination of 'ultralow-fouling' properties demonstrated in the previous section with the superior, durable lubrication validated here establishes these PTB–zwitterionic polymer coatings as a comprehensive solution for enhancing the biocompatibility and functionality of medical interfaces.

The hydration characteristics associated with the different zwitterionic side chains also contribute to the lubrication behaviour of the coatings. For PSBMA, the strongly ionised sulfonate groups promote stable water binding, which helps maintain a hydrated interfacial layer under shear. For PCBMA, the coexistence of carboxylate and quaternary ammonium groups provides electrostatically induced hydration together with possible hydrogen-bonding interactions, contributing to reduced interfacial shear resistance. For PMPC, the phosphorylcholine groups resemble the outer surface chemistry of cell

membranes and can retain water through strong dipole-ion interactions, thereby supporting efficient hydration lubrication. As a result, although the three zwitterionic polymers have different side-chain structures, they all generate highly hydrated interfaces that resist water squeeze-out under compression and shear, leading to stable and low friction coefficients.

To further contextualise the performance of the present coating, we compared our PTB–zwitterionic polymer co-deposited coating with representative antifouling and lubricating coating systems reported in previous studies (Supporting Information S1: Table S2). Although direct quantitative comparison should be interpreted with caution because of differences in substrates, coating thicknesses, counter bodies, applied loads/contact stresses, sliding conditions and fouling models, the comparison highlights the comprehensive advantages of the present system. Unlike some previously reported coatings that mainly focus on either antifouling or lubrication, the coating developed in this work integrates broad-spectrum antifouling performance, ultralow friction, substrate-independent deposition, ultrathin coating geometry and a facile one-step fabrication process.

Despite these promising results, several limitations and future challenges should be noted. The current work mainly evaluates the coatings under in vitro antifouling and tribological conditions, whereas their long-term stability, degradation behaviour and biological responses in complex in vivo environments remain to be systematically investigated. In addition, although the PTB network enables robust and substrate-independent anchoring, the coating stability mainly relies on multiple noncovalent interactions and physical entanglement, and therefore its durability under aggressive wear, sterilisation and long-term implantation conditions should be further assessed. Future work will focus on optimising the coating composition, improving mechanical robustness through mild crosslinking or enhanced interfacial interactions and validating the coatings on practical biomedical devices such as catheters, guidewires, biosensors and artificial joints through comprehensive biocompatibility and in vivo studies.

4 | Conclusion

In summary, we have developed a nanoscale protein-based coating through a facile one-step co-deposition strategy, which exhibits both superior antibiofouling and lubrication properties in physiological environments. Composed of PTB and zwitterionic polymers, the coating enabled stable anchoring on a diverse range of substrates—including metals, inorganic ceramics and hydrophobic polymers—without the need for complex pretreatments. The synergy between the robust anchoring capability of PTB and the high hydration capacity of the zwitterionic polymers endowed the surfaces with exceptional dual functionality: antifouling and lubrication. Specifically, the coating effectively suppressed over 90% of nonspecific adsorption from complex biological media (such as serum, milk and egg white), achieving an 'ultra-low fouling' state. Simultaneously, it facilitated a highly efficient hydration lubrication mechanism under physiological conditions, reducing the coefficient of friction to an ultra-low range of 0.005–0.015. Notably, the integrity of this superior lubrication performance could be preserved even under high contact pressures and during long-term reciprocating wear. This work provides a simple, universal and cost-effective strategy for surface coating construction, offering a promising surface modification solution for implantable medical devices and high-performance biomedical interfaces.

Acknowledgements

The authors thank the financial support from the National Natural Science Foundation of China (Grants 52575203, 52305185 and 52379119).

Conflicts of Interest

The authors declare no conflicts of interest.

Data Availability Statement

The data that support the findings of this study are available from the corresponding author upon reasonable request.

References

1. H. Yuk, J. Wu, and X. Zhao, "Hydrogel Interfaces for Merging Humans and Machines," *Nature Reviews Materials* 7, no. 12 (2022): 935–952, https://doi.org/10.1038/s41578-022-00483-4.

2. Y. Yu, H. Yuk, G. Parada, et al., "Multifunctional "Hydrogel Skins" on Diverse Polymers With Arbitrary Shapes," *Advanced Materials* 31, no. 7 (2019): 9, https://doi.org/10.1002/adma.201807101.

3. Y. Wang, Y. Sun, A. Avestro, P. McGonigal, and H. Zhang, "Supramolecular Repair of Hydration Lubrication Surfaces," *Chem* 8, no. 2 (2022): 480–493, https://doi.org/10.1016/j.chempr.2021.11.001.

4. L. Xiang, J. Zhang, W. Wang, Z. Wei, Y. Chen, and H. Zeng, "Targeted Repair of Super-Lubricating Surfaces via Pairing Click Chemistry," *Advanced Functional Materials* 33, no. 31 (2023): 8, https://doi.org/10.1002/adfm.202301593.

5. Z. Zhao, M. Pan, C. Qiao, et al., "Bionic Engineered Protein Coating Boosting Anti-Biofouling in Complex Biological Fluids," *Advanced Materials* 35, no. 6 (2023): 11, https://doi.org/10.1002/adma.202208824.

6. J. del Rio, O. Henry, P. Jolly, and D. Ingber, "An Antifouling Coating That Enables Affinity-Based Electrochemical Biosensing in Complex Biological Fluids," *Nature Nanotechnology* 14, no. 12 (2019): 1143–1149, https://doi.org/10.1038/s41565-019-0566-z.

7. T. Kang, X. Banquy, J. Heo, et al., "Mussel-Inspired Anchoring of Polymer Loops That Provide Superior Surface Lubrication and Antifouling Properties," *ACS Nano* 10, no. 1 (2016): 930–937, https://doi.org/10.1021/acsnano.5b06066.

8. A. Mutschler, L. Tallet, M. Rabineau, et al., "Unexpected Bactericidal Activity of Poly(arginine)/Hyaluronan Nanolayered Coatings," *Chemistry of Materials* 28, no. 23 (2016): 8700–8709, https://doi.org/10.1021/acs.chemmater.6b03872.

9. H. Vaisocherová, E. Brynda, and J. Homola, "Functionalizable Low-Fouling Coatings for Label-Free Biosensing in Complex Biological Media: Advances and Applications," *Analytical and Bioanalytical Chemistry* 407, no. 14 (2015): 3927–3953, https://doi.org/10.1007/s00216-015-8606-5.

10. R. Zhang, Y. Liu, M. He, et al., "Antifouling Membranes for Sustainable Water Purification: Strategies and Mechanisms," *Chemical Society Reviews* 45, no. 21 (2016): 5888–5924, https://doi.org/10.1039/c5cs00579e.

11. K. Wang, H. Lan, C. Wu, et al., "Electrochemical Polymerization of PEDOT:PSS With Graphene Oxide and Silver Nanoparticles for Antibacterial Coating and SERS Detection," *Surface and Coatings Technology* 485 (2024): 8, https://doi.org/10.1016/j.surfcoat.2024.130889.

12. J. Nakkala, Z. Li, W. Ahmad, K. Wang, and C. Gao, "Immunomodulatory Biomaterials and Their Application in Therapies for Chronic Inflammation-Related Diseases," *Acta Biomaterialia* 123 (2021): 1–30, https://doi.org/10.1016/j.actbio.2021.01.025.

13. S. Wang, Z. Liu, L. Tian, and W. Bing, "Optimisation of Photo-Curable 3D-Printed Bionic Double Layer Lower Extremity Vascular Models Based on Biomechanical Performance Evaluation," *Biosurface and Biotribology* 11, no. 1 (2025): 9, https://doi.org/10.1049/bsb2.70003.

14. X. Zhao, W. Zhao, Y. Zhang, et al., "Recent Progress of Bioinspired Cartilage Hydrogel Lubrication Materials," *Biosurface and Biotribology* 8, no. 3 (2022): 225–243, https://doi.org/10.1049/bsb2.12047.

15. Q. Yu, Z. Wu, and H. Chen, "Dual-Function Antibacterial Surfaces for Biomedical Applications," *Acta Biomaterialia* 16 (2015): 1–13, https://doi.org/10.1016/j.actbio.2015.01.018.

16. H. Huang, C. Zhang, R. Crisci, et al., "Strong Surface Hydration and Salt Resistant Mechanism of a New Nonfouling Zwitterionic Polymer Based on Protein Stabilizer TMAO," *Journal of the American Chemical Society* 143, no. 40 (2021): 16786–16795, https://doi.org/10.1021/jacs.1c08280.

17. C. Jiang, G. Wang, R. Hein, N. Liu, X. Luo, and J. J. Davis, "Antifouling Strategies for Selective in Vitro and in Vivo Sensing," *Chemical Reviews* 120, no. 8 (2020): 3852–3889, https://doi.org/10.1021/acs.chemrev.9b00739.

18. E. Ostuni, R. Chapman, R. Holmlin, S. Takayama, and G. Whitesides, "A Survey of Structure-Property Relationships of Surfaces That Resist the Adsorption of Protein," *Langmuir* 17, no. 18 (2001): 5605–5620, https://doi.org/10.1021/la010384m.

19. S. Jiang and Z. Cao, "Ultralow-Fouling, Functionalizable, and Hydrolyzable Zwitterionic Materials and Their Derivatives for Biological Applications," *Advanced Materials* 22, no. 9 (2010): 920–932, https://doi.org/10.1002/adma.200901407.

20. R. Almousa, X. Wen, S. Na, G. Anderson, and D. Xie, "Hydrophilic Polymer-Coated PVC Surface for Reduced Cell and Bacterial Adhesions," *Biosurface and Biotribology* 8, no. 1 (2022): 34–43, https://doi.org/10.1049/bsb2.12033.

21. R. Almousa, D. Xie, J. Li, and G. Anderson, "Polyvinylchloride Surface Modified With Polymer Brushes for Reduced Protein, Cell and Bacteria Attachment," *Biosurface and Biotribology* 9, no. 4 (2023): 187–198, https://doi.org/10.1049/bsb2.12071.

22. Y. Zhao, X. Zhu, K. Wee, and R. Bai, "Achieving Highly Effective Non-Biofouling Performance for Polypropylene Membranes Modified by UV-Induced Surface Graft Polymerization of Two Oppositely Charged Monomers," *Journal of Physical Chemistry B* 114, no. 7 (2010): 2422–2429, https://doi.org/10.1021/jp908194g.

23. X. Weng, Y. Ji, R. Ma, F. Y. Zhao, Q. F. An, and C. J. Gao, "Superhydrophilic and Antibacterial Zwitterionic Polyamide Nanofiltration Membranes for Antibiotics Separation," *Journal of Membrane Science* 510 (2016): 122–130, https://doi.org/10.1016/j.memsci.2016.02.070.

24. C. Fu, Z. Wang, Y. Gao, et al., "Sustainable Polymer Coating for Stainproof Fabrics," *Nature Sustainability* 6, no. 8 (2023): 984–994, https://doi.org/10.1038/s41893-023-01121-9.

25. Z. Wang, X. Gu, B. Li, et al., "Molecularly Engineered Protein Glues With Superior Adhesion Performance," *Advanced Materials* 34, no. 41 (2022): 9, https://doi.org/10.1002/adma.202204590.

26. X. Wang, Y. Hou, X. Lu, C. Xie, and Y. Jiang, "Protein Hydrogels for Biomedical Applications," *Biosurface and Biotribology* 10, no. 3 (2024): 106–131, https://doi.org/10.1049/bsb2.12084.

27. B. Fang, Q. Ling, W. Zhao, et al., "Modification of Polyethersulfone Membrane by Grafting Bovine Serum Albumin on the Surface of Polyethersulfone/Poly(Acrylonitrile-co-Acrylic Acid) Blended Membrane," *Journal of Membrane Science* 329, no. 1–2 (2009): 46–55, https://doi.org/10.1016/j.memsci.2008.12.008.

28. X. Hu, J. Tian, C. Li, et al., "Amyloid-Like Protein Aggregates: A New Class of Bioinspired Materials Merging an Interfacial Anchor With Antifouling," *Advanced Materials* 32, no. 23 (2020): 11, https://doi.org/10.1002/adma.202000128.

29. H. Ejima, J. Richardson, K. Liang, et al., "One-Step Assembly of Coordination Complexes for Versatile Film and Particle Engineering," *Science* 341, no. 6142 (2013): 154–157, https://doi.org/10.1126/science.1237265.

30. K. Ishihara, "Biomimetic Materials Based on Zwitterionic Polymers Toward Human-Friendly Medical Devices," *Science and Technology of Advanced Materials* 23, no. 1 (2022): 498–524, https://doi.org/10.1080/14686996.2022.2119883.

31. Z. Liu, Y. Zhai, S. Wang, et al., "Polycarboxybetaine in Advanced Drug Delivery Systems: From Structure-Function Relationship to Therapeutic Applications," *International Journal of Pharmaceutics: X* 9 (2025): 13, https://doi.org/10.1016/j.ijpx.2025.100329.

32. L. Ye, Y. Zhang, Q. Wang, et al., "Physical Cross-Linking Starch-Based Zwitterionic Hydrogel Exhibiting Excellent Biocompatibility, Protein Resistance, and Biodegradability," *ACS Applied Materials & Interfaces* 8, no. 24 (2016): 15710–15723, https://doi.org/10.1021/acsami.6b03098.

33. Y. Zhang, J. Zhang, Q. Yang, et al., "Tuning Interfacial Molecular Asymmetry to Engineer Protective Coatings With Superior Surface Anchoring, Antifouling and Antibacterial Properties," *Acta Biomaterialia* 190 (2024): 107–119, https://doi.org/10.1016/j.actbio.2024.10.015.

34. L. Xiang, Y. Zhang, Z. Zhao, et al., "Mechanically Robust, Superlubricating and Antifouling Bilayer Nanocoating for Micro-Bioimplants via a Dual-Function Metal Coordination Approach," *ACS Nano* 19, no. 1 (2024): 1316–1326, https://doi.org/10.1021/acsnano.4c13800.

35. J. Zhang, L. Zhang, X. Cui, et al., "Scalable Polyzwitterion-Polydopamine Coating for Regenerable Oil/Water Separation and Underwater Self-Cleaning of Stubborn Heavy Oil Fouling Without Pre-Hydration," *Chemical Communications* 54, no. 70 (2018): 5–9737, https://doi.org/10.1039/c8cc04611e.

36. H. Willcock and R. O'Reilly, "End Group Removal and Modification of RAFT Polymers," *Polymer Chemistry* 1, no. 2 (2010): 149–157, https://doi.org/10.1039/b9py00340a.

37. Y. Huang, G. Yi, B. Ji, et al., "In Situ One-Pot Synthesis of Polydopamine/Octadecylamine Co-Deposited Coating in Capillary for Open-Tubular Capillary Electrochromatography," *Journal of Chromatography A* 1610 (2020): 9, https://doi.org/10.1016/j.chroma.2019.460559.

38. D. Meng, Y. Li, P. Qi, et al., "Constructing a Bio-Based Flame-Retardant Coating Through Co-Depositing Polydopamine and Guanosine 5′-Monophosphate Disodium Salt (GMP) for Flexible Polyurethane Foam," *Materials Today Chemistry* 27 (2023): 12, https://doi.org/10.1016/j.mtchem.2022.101320.

39. M. Zhang, L. Jin, Y. Zhai, et al., "Bio-Inspired Gallic Acid-Gelatin Coating: A Novel Strategy for Eco-Friendly Interfacial Modification of Carbon Fiber Composites," *Composites Communications* 26 (2021): 6, https://doi.org/10.1016/j.coco.2021.100790.

40. L. Liu, H. Shi, H. Yu, R. Zhou, J. Yin, and S. Luan, "One-Step Hydrophobization of Tannic Acid for Antibacterial Coating on

Catheters to Prevent Catheter-Associated Infections," *Biomaterials Science* 7, no. 12 (2019): 5035–5043, https://doi.org/10.1039/c9bm01223k.

41. A. Karkooti, M. Rastgar, N. Nazemifard, and M. Sadrzadeh, "Study on Antifouling Behaviors of GO-Modified Nanocomposite Membranes Through QCM-D and Surface Energetics Analysis," *Colloids and Surfaces A: Physicochemical and Engineering Aspects* 588 (2020): 13, https://doi.org/10.1016/j.colsurfa.2019.124332.

42. D. Tintor, K. Ninkovic, J. Milosevic, and N. Polovic, "Gaining Insight into Protein Structure via ATR-FTIR Spectroscopy," *Vibrational Spectroscopy* 134 (2024): 8, https://doi.org/10.1016/j.vibspec.2024.103726.

43. A. R. Cooper and D. S. Van Derveer, "Recent Advances in Aqueous Gel-Permeation Chromatography," *Journal of Liquid Chromatography* 1, no. 5 (1978): 693–726, https://doi.org/10.1080/01483917808060027.

44. D. Castner, K. Hinds, and D. Grainger, "X-Ray Photoelectron Spectroscopy Sulfur 2p Study of Organic Thiol and Disulfide Binding Interactions With Gold Surfaces," *Langmuir* 12, no. 21 (1996): 5083–5086, https://doi.org/10.1021/la960465w.

45. L. Carr, H. Xue, and S. Jiang, "Functionalizable and Nonfouling Zwitterionic Carboxybetaine Hydrogels With a Carboxybetaine Dimethacrylate Crosslinker," *Biomaterials* 32, no. 4 (2011): 961–968, https://doi.org/10.1016/j.biomaterials.2010.09.067.

46. X. Song, J. Man, Y. Qiu, et al., "Study of Hydration Repulsion of Zwitterionic Polymer Brushes Resistant to Protein Adhesion through Molecular Simulations," *ACS Applied Materials & Interfaces* 16, no. 14 (2024): 17145–17162, https://doi.org/10.1021/acsami.3c18546.

47. Z. Zhao, C. Huang, and H. Zeng, "Zwitterion-Conjugated Protein Coatings for Enhanced Antifouling in Complex Biofluids: Underlying Molecular Interaction Mechanisms," *Langmuir* 40, no. 48 (2024): 25708–25716, https://doi.org/10.1021/acs.langmuir.4c03975.

48. L. Han, Y. Tan, C. Xu, T. Xiao, T. A. Trinh, and J. W. Chew, "Zwitterionic Grafting of Sulfobetaine Methacrylate (SBMA) on Hydrophobic PVDF Membranes for Enhanced Anti-Fouling and Anti-Wetting in the Membrane Distillation of Oil Emulsions," *Journal of Membrane Science* 588 (2019): 13, https://doi.org/10.1016/j.memsci.2019.117196.

49. A. Galuza, V. Kiseliov, I. Kolenov, A. Belyaeva, and Y. Kuleshov, "Developments in THz-Range Ellipsometry: Quasi-Optical Ellipsometer," *IEEE Transactions on Terahertz Science and Technology* 6, no. 2 (2016): 183–190, https://doi.org/10.1109/tthz.2016.2525732.

50. L. Zhou, M. Cai, T. Tong, and H. Wang, "Progress in the Correlative Atomic Force Microscopy and Optical Microscopy," *Sensors* 17, no. 4 (2017): 15, https://doi.org/10.3390/s17040938.

51. A. Asha, Y. Chen, and R. Narain, "Bioinspired Dopamine and Zwitterionic Polymers for Non-Fouling Surface Engineering," *Chemical Society Reviews* 50, no. 20 (2021): 11668–11683, https://doi.org/10.1039/d1cs00658d.

52. W. Yang, M. Pan, J. Zhang, et al., "A Universal Strategy for Constructing Robust and Antifouling Cellulose Nanocrystal Coating," *Advanced Functional Materials* 32, no. 8 (2022): 12, https://doi.org/10.1002/adfm.202109989.

53. A. Wang, E. Dillon, S. Maharjan, et al., "Resolving Nanocomposite Interfaces via Simultaneous Submicrometer Optical-Photothermal Infrared-Raman Microspectroscopy," *Advanced Materials Interfaces* 8, no. 5 (2021): 8, https://doi.org/10.1002/admi.202001720.

54. C. Lima, H. Muhamadali, Y. Xu, M. Kansiz, and R. Goodacre, "Imaging Isotopically Labeled Bacteria at the Single-Cell Level Using High-Resolution Optical Infrared Photothermal Spectroscopy," *Analytical Chemistry* 93, no. 6 (2021): 3082–3088, https://doi.org/10.1021/acs.analchem.0c03967.

55. Y. Su, X. Hu, H. Tang, et al., "Steam Disinfection Releases Micro (Nano)plastics From Silicone-Rubber Baby Teats as Examined by Optical Photothermal Infrared Microspectroscopy," *Nature Nanotechnology* 17, no. 1 (2022): 76–85, https://doi.org/10.1038/s41565-021-00998-x.

56. A. Marchetti, V. Beltran, G. Nuyts, et al., "Novel Optical Photothermal Infrared (O-PTIR) Spectroscopy for the Noninvasive Characterization of Heritage Glass-Metal Objects," *Science Advances* 8, no. 9 (2022): 9, https://doi.org/10.1126/sciadv.abl6769.

57. H. Wang, J. Song, and Y. Liu, "Superlubricity of Double-Network Hydrogels Modified With Tween 80 and Hydrogenated Soybean Phosphatidylcholine," *Biosurface and Biotribology* 11, no. 1 (2025): 11, https://doi.org/10.1049/bsb2.70008.

58. Z. Yang, W. Jiang, H. Yan, et al., "Tribological Properties of Ti-Based Nanofiber-CS Composite Flexible Coatings," *Biosurface and Biotribology* 11, no. 1 (2025): 8, https://doi.org/10.1049/bsb2.70001.

59. G. Chapman and G. Cokelet, "Flow Resistance and Drag Forces Due to Multiple Adherent Leukocytes in Postcapillary Vessels," *Biophysical Journal* 74, no. 6 (1998): 3292–3301, https://doi.org/10.1016/s0006-3495(98)78036-1.

60. N. Mazarevica, Y. Chen, K. Ren, H. J. Kaper, B. D. Monnery, and P. K. Sharma, "Influence of Neutral and Cationic Phytoglycogen Nanoparticles on Cartilage and Ocular Lubrication," *Biosurface and Biotribology* 11, no. 1 (2025): 12, https://doi.org/10.1049/bsb2.70002.

61. W. Lin and J. Klein, "Hydration Lubrication in Biomedical Applications: From Cartilage to Hydrogels," *Accounts of Materials Research* 3, no. 2 (2022): 213–223, https://doi.org/10.1021/accountsmr.1c00219.

Supporting Information

Additional supporting information can be found online in the Supporting Information section.

Supporting Information S1: bsb270029-sup-0001-suppl-data.docx.